Two-frequency fiber-optic sensor system using high-birefringence optical fiber

Pie-Yau Chien and Ci-Ling Pan

A fiber sensor system based on high-birefringence optical fiber and a frequency-stabilized He–Ne Zeeman laser ($\lambda = 0.6328$ μm) has been demonstrated. The small path-length changes of interest are extracted from the amplitude or phase of the laser beat frequency by using either the phase-sensitive detection or the phase-demodulation technique. A minimum detectable optical phase delay of 1.5×10^{-6} rad/Hz$^{1/2}$ or 17×10^{-6} rad/Hz$^{1/2}$ has been achieved.

Key words: high-birefringence fiber sensor.

Introduction

The fiber-optic Mach–Zehnder interferometer has been widely used for sensor applications.[1] The incorporation of pigtailed laser diodes and fiber couplers has facilitated the development of the all-fiber Mach–Zehnder interferometer. Recently, high-birefringence fiber was also developed successfully and was used to demonstrate various fiber-optic components, e.g., fiber polarizers,[2,3] depolarizers,[4,5] fiber couplers,[6] optical filters,[7,8] and optical isolators.[9] Alternatively, single-arm fiber interferometers (polarimeters)[10–12] based on high-birefringence fiber have also been implemented, which offer several advantages over the two-arm Mach–Zehnder interferometers, e.g., simplicity in design, enhanced immunity to environmental noise, and potentially higher sensitivity than a two-arm interferometer. The interference signal in this system results from mixing two polarization eigenmodes in high-birefringence optical fiber.

In this paper a single-arm fiber interferometer that uses a high-birefringence optical fiber and a He–Ne Zeeman laser as the light source is demonstrated. A comparative study of the two possible optical phase detection methods for optical heterodyne detection, phase-sensitive detection (PSD) and phase demodulation (PD), in our single-arm optical fiber interferometer are reported. This optical heterodyne technique[13,14] has also been used to detect the induced optical phase delay in two-arm interferometers. Our approach is based on adjusting the two linearly polarized light outputs from the Zeeman laser such that they are at an angle of 0° or 45° to the principal axes of the high-birefringence fiber. The induced optical phase change in the single-arm interferometer can then be extracted from the phase or the amplitude of the beat frequency of the Zeeman laser. By using this technique, we can process the low-frequency signal of interest at a relatively high beat frequency, so that the unwanted low-frequency noise may be eliminated. A phase bias servo loop was also adopted to minimize the optical phase drift that is due to environmental noise. A minimum detectable optical phase delay of 1.5 μrad within 1.0-Hz bandwidth can be readily achieved with the PSD technique.

Basic Principles

Figure 1 illustrates the basic operating principle of the single-arm optical fiber interferometer. The output of a longitudinal Zeeman He–Ne laser consists of two mutually perpendicular, circularly polarized components of frequencies ω_1 and ω_2. A $\lambda/4$ plate is used to convert these into the desired orthogonally linear polarized states. The laser beam is then focused into a high-birefringence optical fiber. The two polarization components propagate with different phase velocities that are determined by the refractive indices n_x and n_y along the two principal axes of the fiber, respectively. The phase delay between these two fiber modes is

$$\phi = K_0(n_x - n_y)L, \tag{1}$$

where $K_0 = 2\pi/\lambda_0$ is the free-space wave vector, λ_0 is the wavelength of light in free space, and L is the fiber length.

The authors are with the Institute of Electro-Optical Engineering, National Chiao-Tung University, Hsinchu, Taiwan 30050, China.

Received 1 May 1990.
0003-6935/92/101407-05$05.00/0.

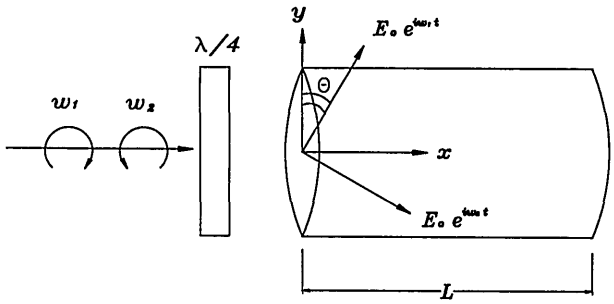

Fig. 1. Configuration of a high-birefringence optical fiber sensor based on a two-frequency light source.

These two orthogonal linearly polarized modes are assumed to be of the same amplitude E_0 and focused into the optical fiber with the plane of polarization at an angle of θ to the principal axes of the optical fiber. We further assume that the two polarization eigenmodes remain uncoupled within the fiber length. After exiting the optical fiber, the field components polarized along the principal axes are

$$E_{sx}(L) = E_0 \sin\theta \exp[i(\omega_1 t + \phi_x)] + E_0 \cos\theta \exp[i(\omega_2 t + \phi_x)], \tag{2a}$$

$$E_{sy}(L) = E_0 \cos\theta \exp[i(\omega_1 t + \phi_x)] - E_0 \sin\theta \exp[i(\omega_2 t + \phi_y)], \tag{2b}$$

where ω_1 and ω_2 are the angular frequencies of the laser output, $\phi_x = K_0 n_x L$, and $\phi_y = K_0 n_y L$. After traversing a polarizer with its axes at an angle of 45° to $E_{sx}(L)$ and $E_{sy}(L)$, the interference signal as represented by the photocurrent of the photodetector can be written as

$$\begin{aligned} I(t) &= (E_{sx}/\sqrt{2} + E_{sy}/\sqrt{2})(E_{sx}/\sqrt{2} + E_{sy}/\sqrt{2})^* \\ &= E_0^2 + E_0^2 \cos^2\theta \cos[(\omega_1 - \omega_2)t + \phi] \\ &\quad - E_0^2 \sin^2\theta \cos[(\omega_1 - \omega_2)t - \phi], \end{aligned} \tag{3}$$

where $\phi = \phi_x - \phi_y$. The E_0 term in Eqs. (2) can be removed by using an ac-coupled optical receiver. Equation (3) reduces to

$$I(t) = I_0 \cos[(\omega_1 - \omega_2)t \pm \phi] \quad \text{for } \theta = 0 \text{ or } \pi/2, \tag{4a}$$

$$I(t) = I_0 \sin\phi \sin[(\omega_1 - \omega_2)t] \quad \text{for } \theta = \pi/4 \text{ or } -\pi/4, \tag{4b}$$

where $I_0 = \alpha|E_0|^2$ is the intensity of light, α is a constant that takes into account the coefficient of the photodetector response. From Eqs. (4a) and (4b) we can draw the following conclusions:

(1) The induced optical phase shift ϕ in high-birefringence optical fiber can be extracted from the phase term at the beat frequency $|\omega_1 - \omega_2|$, as shown in Eq. (3a), or the amplitude term at the beat frequency, as shown in Eq. (3b), by selecting the angle θ.

(2) The optical phase delay ϕ in Eqs. (3a) and (3b) can be obtained by employing the PD to demodulate the phase term or the PSD to demodulate the amplitude term. A comparison of the accuracy of these two detection methods can be implemented in our interferometer.

Experimental Method

A schematic diagram of our experimental setup is shown in Fig. 2. The output of a frequency-stabilized longitudinal He–Ne Zeeman laser was first converted into two orthogonal linearly polarized components by a $\lambda/4$ plate. The axes of the two linear polarization states can be rotated by rotating the optical axis of the $\lambda/4$ plate. The beat frequency, $|\nu_1 - \nu_2|$, of the Zeeman laser was stabilized to $\Delta|\nu_1 - \nu_2| \leq 100$ Hz (Refs. 15 and 16) over a 2-h period with $|\nu_1 - \nu_2| = 560$ kHz for our laser. This corresponded to a frequency stability of $\Delta\nu_{1,2}/\nu_{1,2} \leq 2.0 \times 10^{-10}$. An optical isolator was used to eliminate the light reflected into the laser cavity. A microscope objective lens of 10× then focused the laser beam into the optical fiber. The optical fiber was a high-birefringence type at 0.63 μm with a beat length of 2.0 mm. The fiber length was 5.0 m and this was wound onto two 2-cm-diameter cylindrical piezoelectric transducers (PZT's), PZT1 and PZT2. PZT1 was used for signal simulation, and PZT2 provided a voltage-controlled phase delay for optical phase bias stabilization.

The light from the output end of the fiber was analyzed by a Glan–Thompson polarizer and detected by a silicon photodetector that was biased at 15 V. The photocurrent of the detector was passed through a 10-kΩ loading resistor and the signal at the loading resistor was then amplified by an ac-coupled video amplifier. An oscilloscope was used to monitor the output of the video amplifier. Either a PD (phase meter) or a PSD (lock-in) circuit was used to demodulate the optical phase delay.

The linear polarization states of the input light were rotated through the $\lambda/4$ plate with an angle of 0° or 90° with respect to the principal axes of the optical fiber. The Glan–Thompson polarizer was adjusted at 45° with respect to the principal axes of the exiting optical fiber. A sinusoidal signal of 1.0 kHz was applied to PZT1 to simulate change in the optical phase delay.

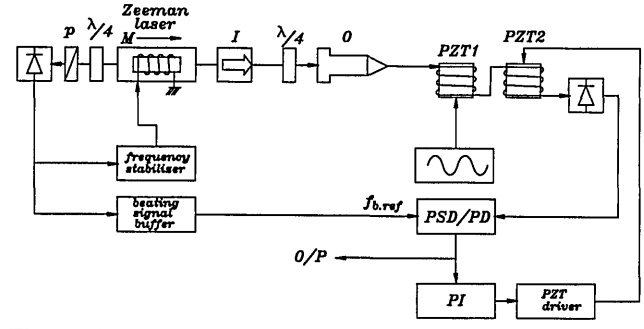

Fig. 2. Experimental setup of the single-arm high-birefringence optical fiber sensor system: P, polarizer; I, isolator; O, objective lens; PZT, piezoelectric transducer; PSD, phase-sensitive detector; PD, phase demodulator (phase meter); PI, proportional and integrating circuits.

Results and Discussions

The beat signal from the He–Ne Zeeman laser and the signal at the output of the video amplifier are shown in Figs. 3(a) and 3(b) with the interferometer at different optical bias points. It can be seen that the optical phase variations were present in the phase term of the signal at the beat frequency, as shown in Eq. (4a). If the $\lambda/4$ plate were rotated $\pm 45°$ with respect to the principal axes of the optical fiber and other conditions were the same as in the above experiment, we found that the optical phase variation was present in the amplitude term of the interference signal at the beat frequency, as shown in Eq. (4b). Figures 4(a) and 4(b) show results for different simulation signals applied to PZT1 and the output signal at the video amplifier.

To eliminate the optical phase fluctuations induced by environmental disturbances, a servo loop was used for phase bias point stabilization. It was implemented by nulling the low-frequency drift in the interference signal detected at the output of either the PD or the PSD circuit. The error signal was fed through proportional and integrating (PI) compensating circuits to control the fiber length by using PZT2. When the servo loop was closed, the optical phase bias ϕ_o was stabilized at $\phi_o = 0$. These results are shown in Fig. 5 for the PD technique and in Fig. 6 for the PSD technique. With the servo loop closed, a 5-kHz sinusoidal signal that corresponds to a phase delay of ~ 100 μrad was applied to PZT1 to test system performance. We can successfully demodulate the optical phase delay by either the PD or PSD method. These results are shown in Fig. 7(a) for the PD technique and in Fig. 7(b) for the PSD technique.

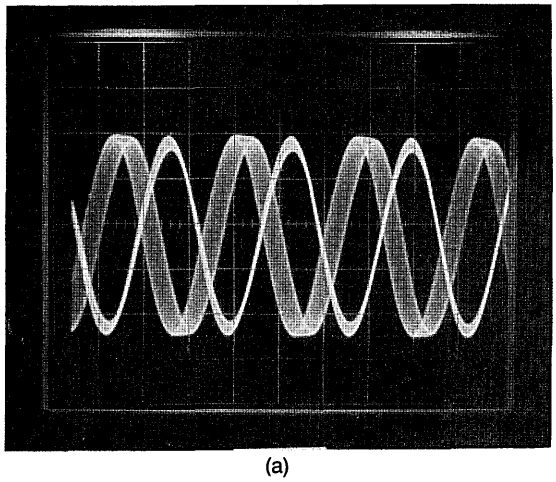

(a)

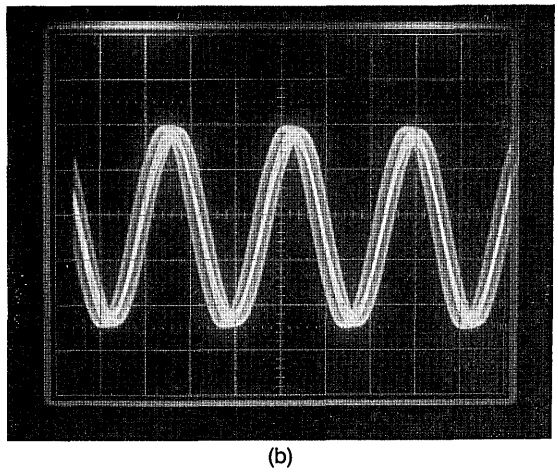

(b)

Fig. 3. Output beat signal of 560 kHz at a photodetector output of $\theta = 0°$. Here a 1.0-kHz sinusoidal signal was applied to PZT1. The optical phase delay was present in the phase term of the beat signal: (a) phase stabilization loop open; (b) phase stabilization loop closed.

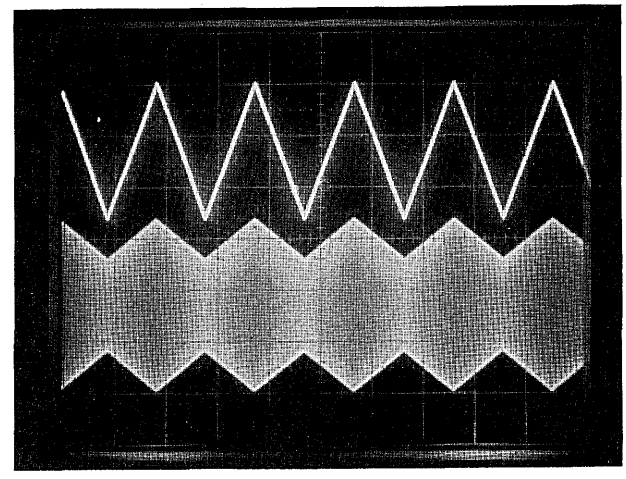

(a)

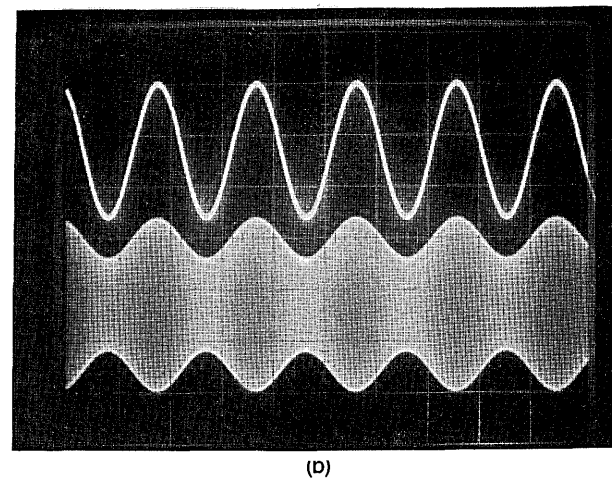

(b)

Fig. 4. Output signal at the photodetector for $\theta = 45°$ with different signals applied to PZT1. In this case, information on the optical phase delay was in the amplitude of the beat signal. The upper trace represents the applied signal; the lower trace represents the photodetector output signal. The applied signal was at 1.0 kHz. The applied signal is (a) a triangular waveform (b) a sinusoidal waveform.

To estimate the ultimate sensitivity, ϕ_{min}, of our interferometer, it is necessary to compare the theoretical signal-to-noise ratio with that actually measured. For the experiment reported here, $P = 0.1$ mW, the noise bandwidth $B = 1$ Hz, the quantum efficiency of the photodetector is $\eta = 0.5$, and $\lambda = 6328$ nm, we obtain $\phi_{min} = (4hcB/\lambda\eta P)^{1/2} \cong 0.2$ μrad. The long-term optical phase delay fluctuations may result from

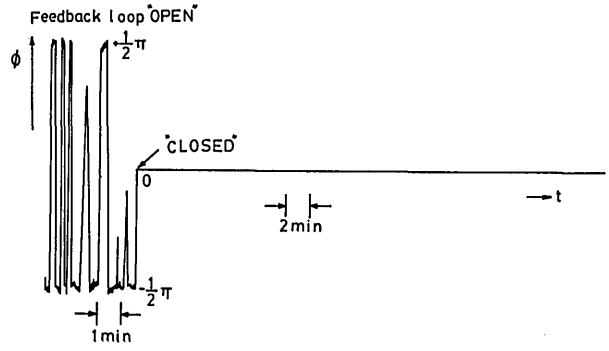

Fig. 5. Output signal of the PD for $\theta = 0°$ with the servo loop free running and closed. The peak-to-peak phase variations of the signal in the free-running condition correspond to a phase change of πrad.

the frequency drift of the Zeeman laser. This can be estimated from $\Delta\phi = [2\pi(n_x - n_y)L/c] \times \Delta\mu \cong 3.0$ μrad. This is an order of magnitude higher than the phase noise that is due to the shot noise limit in our system.

The phase delay bias in our system can be stabilized to within 1.5 μrad with a 1.0-Hz bandwidth in the PSD method. To demonstrate, we applied a $>\pi$rad phase fluctuation to the system when the system was free running. The demodulated output signal of the PSD circuit exhibited peak-to-peak variations that correspond to the phase change of πrad. This value was ± 4.5 V as shown in Fig. 6. When the servo loop was closed, the phase fluctuation was stabilized to within 50 μV. Since the bandwidth of our servo loop was 400 Hz, the minimum detectable phase delay ϕ_{min} was of the order of 1.5 μrad/Hz$^{1/2}$. This result is 1 order of magnitude higher than the shot-rise-limited detectable optical phase but lower than the long-term optical phase fluctuations induced by laser frequency drift. The same experimental procedure was also applied for the PD detection scheme. In this method, the resolution of the phase meter circuit is ~ 17 μrad/Hz$^{1/2}$. This is due to the pulse width modulation characteristics of the PD circuit; it is 1 order of magnitude higher than that achievable by the PSD method.

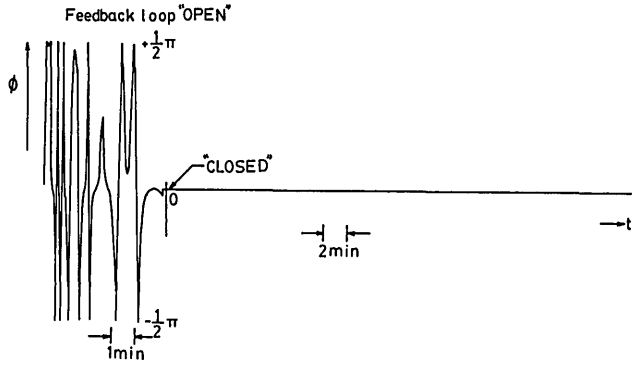

Fig. 6. Output signal of the PSD for $\theta = 45°$ with the servo loop free running and closed. The peak-to-peak phase variations in the free-running condition correspond to a phase change of πrad.

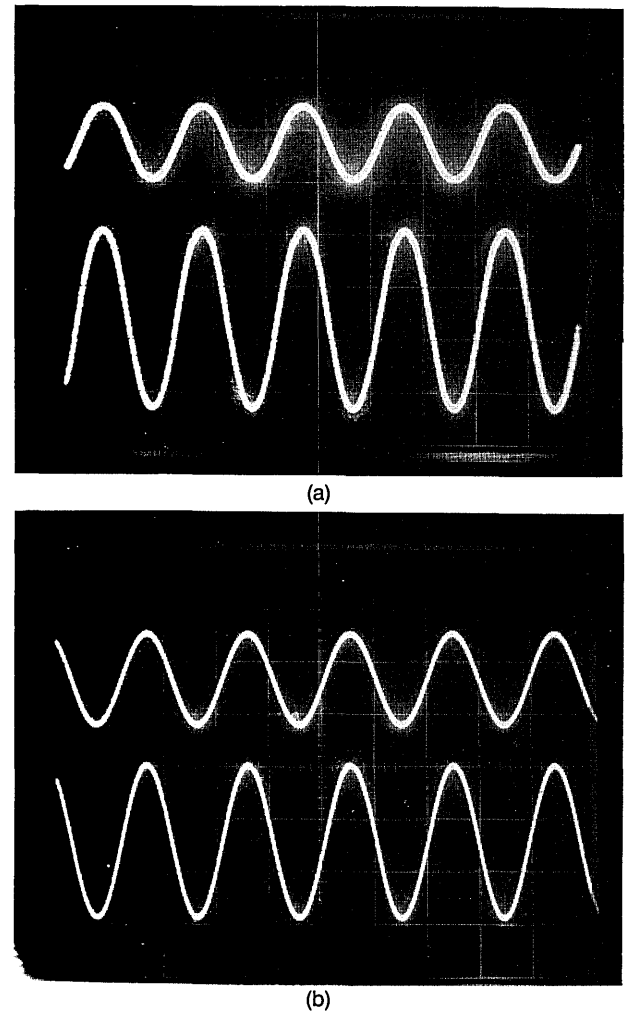

Fig. 7. Applied 5.0-kHz simulation signal and the demodulated output signal with the phase meter PD of the PSD method. The upper trace represents the demodulated output signal; the lower trace represents the signal applied to PZT1: (a) the PD method; (b) the PSD method.

It is interesting to compare the linearity of the scale factor of our interferometer for the two detection methods. In the PSD method, the output signal is proportional to $I_0 \sin\phi$. Two problems concerning the scale factor are apparent: (1) It is a nonlinear function of the optical phase delay ϕ, except when ϕ is small, e.g., $\phi \leq \pi/4$. In that case, the output can be written as $I(t) = I_0\phi$. In the PD method, however, the PD circuit output is linearly proportional to the optical phase delay. The linear dynamic range of the phase measured in the PD method is from -2π to $+2\pi$. (2) When the PSD method is used, the output signal depends on I_0. Thus the fluctuations of the laser output and the polarization state of the two interfering light components will cause a change in I_0. In the PD method, the I_0 term can be eliminated by changing the sinusoidal output waveform to the square waveform. It follows that the linearity and the dynamic range of the scale factor of the PD method are superior to those of the PSD method. The sensitivity

of the PD method is, however, lower than that of the PSD method.

Conclusion

A phase-bias-stabilized, single-arm, high-birefringence, fiber-optic interferometric sensor system based on a frequency-stabilized He–Ne Zeeman laser has been demonstrated and characterized. Two demodulation methods for obtaining optical phase delays have been compared in detail. Minimum detectable phase delays of 1.5 and 17.0 $\mu rad/Hz^{1/2}$ have been obtained by the PSD and PD methods, respectively. An attractive feature of this single-arm, fiber-optic interferometer is its simplicity and improved fiber sensitivity, which suggests that the single-arm, optical fiber interferometer can be competitive with a conventional two-arm, fiber-optic, Mach–Zehnder interferometer.

This work was partially supported by the National Science Council of the Republic of China under grant NSC 79-0417-E009-02.

References

1. T. G. Giallorenzi, J. A. Bucaro, A. Dandridge, G. H. Sigel, Jr., J. H. Cole, S. C. Rashleigh, and R. G. Priest, "Optical fiber sensor technology," IEEE J. Quantum Electron. **QE-18,** 626–665 (1982).
2. M. P. Varnham, D. N. Payne, A. J. Barlow, and E. J. Tarbox, "Coiled-birefringent-fiber polarizers," Opt. Lett. **9,** 679–680 (1983).
3. K. Okamoto, "Single-polarization operation in high birefringent optical fibers," Appl. Opt. **23,** 2638–2642 (1984).
4. K. Bohm, K. Peterman, and E. Weidel, "Performance of Lyot depolarizer with birefringent single-mode fibers," IEEE J. Lightwave Technol **LT-1,** 71–74 (1983).
5. K. Mochizuki, "Degree of polarization in jointed fibers: the Lyot depolarizer," Appl. Opt. **23,** 3284–3288 (1984).
6. B. K. Nayar and D. R. Smith, "Monomode-polarization-maintaining fiber directional coupler," Opt. Lett **8,** 543–545 (1983).
7. Y. Yeh and R. Ulrich, "Birefringent optical fibers in single-mode fiber," Opt. Lett. **6,** 278–280 (1981).
8. K. Okamoto and J. Noda, "Spectral band-elimination filter consisting of concatenated dual-core fibers," Electron. Lett. **22,** 211–212 (1986).
9. G. W. Day, D. N. Payne, A. J. Barlow, and J. J. Ramskov-Hansen, "Faraday rotation in coiled, monomode optical fibers: isolators, filters, and magnetic sensors," Opt. Lett **7,** 238–240 (1982).
10. M. P. Varnham, A. J. Barlow, D. N. Payne, and K. Okamoto, "Polarimetric strain gauges using high birefringent fibers," Electron Lett. **19,** 699–701 (1983).
11. M. D. Mermelstein, "High-birefringent fiber-optic polarimeter with submicroradian phase delay sensitivity," IEEE J. Lightwave Technol. **LT-4,** 449–453 (1986).
12. D. Chardon and S. J. Huard, "A new interferometric and polarimetric temperature optical fiber sensor," IEEE J. Lightwave Technol. **LT-4,** 720–725 (1986).
13. N. Nokes, B. C. Hill, and A. E. Barell, "Fiber optical heterodyne interferometer for vibration measurement in biological system," Rev. Sci. Instrum. **49,** 722–728 (1978).
14. P. R. Forman and F. C. Jahoda, "Linear birefringence effects on fiber-optic current sensors," Appl. Opt. **27,** 3088–3096 (1988).
15. T. Baer, F. V. Kowalski, and J. L. Hall, "Frequency stabilization of a 0.633-μm longitudinal Zeeman laser," Appl. Opt. **19,** 3137–3140 (1980).
16. C. L. Pan and P.-Y. Chien, "Simultaneous output power and frequency stabilization of a Zeeman He–Ne laser," Appl. Opt. **25,** 1375–1376 (1986).